Authors' Response to Reviews of

The tidal effects in the Finite-volumE Sea ice–Ocean Model (FESOM2.1): a comparison between parameterised tidal mixing and explicit tidal forcing

Pengyang Song et al.
Geosci. Model Dev. Discuss., 10.5194/gmd-2022-25

RC: ***Reviewers' Comment***, AR: Authors' Response, ☐ Manuscript Text

Dear editor and reviewers,

Thanks for the comments on our manuscript. By improving our work and revising our paper following the reviewers' guidance, we found that our last responses to some reviewers' comments are not sufficient. Thus, we want to add some responses to the reviewers' comments to better explain and improve our work.

Yours sincerely,

Pengyang Song et al.

1. Reviewers' comments

RC: ***It is unclear how the tidal motion in LSTIDE leads to vertical mixing, i.e. larger vertical diffusivity.***

AR: The model applies the KPP scheme, in which vertical shear is decisive to the mixing in the interior of the ocean. Thus, we thought the vertical mixing in LSTIDE is contained with the vertical shear of baroclinic tides.

However, by plotting the meridional transection of the vertical diffusivity from the model results, we found that vertical diffusivity is not significantly changed. The reason is that the model resolution can hardly simulate propagating internal tides, so is the vertical shear from internal tides. By studying how the upwelling occurs at the Kuril–Aleutian Ridge, we realised that the direct tide–topography interaction affects the along-boundary upwelling via the turbulent buoyancy flux. Referring to the Reynolds stress equation, the vertical diffusivity coefficient represents the strength of the turbulent buoyancy flux, which cannot be resolved by the model (Appendix A2 in the revised manuscript). But LSTIDE simulates tidal motions in the model and shows intense turbulent buoyancy flux at the Kuril–Aleutian Ridge, equal to enhancing vertical diffusivity in the model (Fig. 4). The equivalent vertical diffusivity caused by turbulent buoyancy fluxes can reach $10^{-2}\ m^2\ s^{-1}$. Unlike CVTIDE that assumes tidal mixing decaying from bottom to top, in LSTIDE the upwelling caused by turbulent buoyancy flux only occurs at near-bottom layers. That explains why the PMOC pattern in the North Pacific (Fig. 5f) coincides well with the bathymetry. The pattern of tide-induced upwelling which occurs near bottom also agrees with the argument raised in Ferrari et al. (2016).

Ferrari, R., Mashayek, A., McDougall, T. J., Nikurashin, M., & Campin, J. M. (2016). Turning ocean mixing upside down. Journal of Physical Oceanography, 46(7), 2239-2261.

RC: ***In Figs 3-6 the hydrography in the simulations is compared to the observationally based data set WOA18. The results are mixed, and the differences between the different simulations are generally small compared to the bias of the control simulation. It is clear that neither CVTIDE nor LSTIDE gives any decisive improvement, and the improvements that exist in some regions may well be for the wrong rea-***

son. For example, biases caused by the background diffusivity, the K-profile parameterisation or the GM-parameterisation might be compensated by the parameterisation of tidal mixing. It is therefore difficult to draw any conclusion at all from these figures. CVTIDE and LSTIDE should instead be regarded as sensitivity tests, and the interesting question is not whether they decrease the bias, but how they modify the hydrography compared to NOTIDE.

AR: Below Fig. 1 and Fig. 2 show the meridional transection plot of hydrography and vertical diffusivity in the Atlantic Ocean and the Pacific Ocean. We can see from Figs. 1d, 1e, 2d and 2e that CVTIDE affects the ocean by enhancing the mixing in the interior ocean. Thus the patterns mainly feature two layers. Take ocean temperature as an example, a direct explanation is that with mixing enhanced in the ocean, the upper ocean would be cooler and the deeper ocean would be warmer. But this is different for LSTIDE, because LSTIDE does not introduce enough mixing. The hydrography in LSTIDE is also changed significantly due to the strengthening of PMOC–AMOC cycle. This is also the main finding of our work. In Fig. 2g, the reduction of temperature biases in NOTIDE is evident. And from our result, we think that with the vertical mixing scheme treated properly, the hydrography biases would be reduced via both interior mixing (like CVTIDE) and the adjustment of the MOC (like LSTIDE). That is why we talk about reducing the biases.

RC: ***The key to understanding the effect on hydrography is the vertical diffusivity. Its geographical distribution is shown in Fig 12, but this should be complemented by plots with the vertical profile of the diffusivity, along with the vertical hydrographic profiles.***

AR: Below Fig. 1 and Fig. 2 show the transection plot of hydrography and vertical diffusivity in the Atlantic Ocean and the Pacific Ocean. These figures lead to the same conclusions as the figures we show in our manuscript. Therefore, we think it's better not to add too much redundant information to the manuscript.

RC: ***To explain the increased strength of the overturning cell in the North Pacific, the authors invoke the increased vertical diffusivity at the Kuril Ridge and Aleutian Ridge seen in Fig 12l and probably caused by trapped internal tides. This might be correct, but no strong support for this explanation is shown. Here are some problems. i) According to Fig 12 the vertical diffusivity in the Northern Pacific increases much more in CVTIDE than in LSTIDE, and yet there is much less upwelling in CVTIDE. In order to make the explanation credible, the pattern of vertical diffusivity (geographical and vertical) in the Northern Pacific should be studied in detail. ii) The strong diffusivity could be caused by resonant trapped waves, but it could also be caused simply by strong shear of the barotropic tide caused by bottom friction on the continental shelf. It should be possible to check which alternative is correct.***

AR: Thanks again for this comment. In the model, vertical diffusivity coefficient (K_v) is dependent on the vertical shear. If the bottom friction provides strong vertical shear near the bottom, we should find evidence of larger vertical diffusivity along the ocean bottom. But we can see from the section plot of K_v (Fig. 4c) that no significant change emerges in LSTIDE. This is because that the tidal velocity in deep ocean is not as large as in shallow ocean. Indeed, we agree that on continental shelves the bottom friction is strong and the strong vertical shear should increase bottom K_v via enhanced vertical shear. However, this does not coincide with the upwelling in the North Pacific from 4000 m to 1000 m. Therefore, we rule out this possibility.

By checking the meridional transection plots of the vertical diffusivity and the turbulent buoyancy flux, we found that LSTIDE increases PMOC upwelling by introducing turbulent buoyancy flux instead of increasing K_v. The Appendix A2 of our revised manuscript explains that these two approaches are equivalent. If we also consider the equivalent vertical diffusivity caused by the turbulent buoyancy flux, we can find that the increase of vertical diffusivity in LSTIDE is much stronger than CVTIDE and is more concentrated at the near-bottom layers. That is why CVTIDE does not show the same changes as LSTIDE regarding the strength and shape of the North Pacific MOC cell.

RC: ***In section 5.2 it is argued that the stronger AMOC in LSTIDE is caused by increased upwelling in North Pacific and the Indonesian Archipelago. This seems far-fetched. An alternative explanation is that it is caused by increased vertical diffusivity in upper 3000 m of the Atlantic itself, but this is difficult to judge since vertical diffusivity profiles are not shown.***

AR: We plot the Atlantic meridional section of vertical diffusivity in below Fig. 3. Our results do not show evidence of stronger vertical diffusivity in the mid- and low-latitude Atlantic Ocean in LSTIDE. Note that in high-latitude North Atlantic Ocean the large vertical diffusivity is applied for gravitational instability (deep convection). Thus, we don't think this should be the reason for a stronger AMOC in LSTIDE.

Another evidence to prove that the stronger AMOC in LSTIDE is not caused by the mixing in the Atlantic is that the pattern of AMOC difference does not show closed overturning circulation (streamfunction lines) in the mid-latitude Atlantic (Fig. 5e). If the the mixing in the Atlantic itself would explain the strengthening of the AMOC, the upwelling should happen in the Atlantic. However, we can only see a closed circulation pattern in the North Atlantic (20° N–40° N) with a strength of 0.5 Sv. This cannot explain the rest 1.5 Sv, which is the strength of the upper south-to-north flow and the lower north-to-south flow at the 30° S Atlantic.

RC: ***The energy diagnostics in Table 3 are potentially interesting, but unfortunately incomplete. The surface energy input, bottom drag, viscous dissipation, buoyancy flux and barotropic tide power are terms in the budget for kinetic energy. However, the budget is far from closed, particularly in LSTIDE. (Note that the sign of the buoyancy flux should be changed when calculating the budget, since a positive*** ρw ***is a conversion from kinetic energy to potential energy, i.e. a sink of kinetic energy.) It is striking that the barotropic tide power in LSTIDE is much larger than the increase of the sinks. The main missing term is probably energy loss due to horizontal viscosity, which should therefore also be diagnosed. If there are no more missing terms, the remaining residual will then be due to numerical errors. This is essential to know.***

AR: Thanks again for pointing out this. We checked each term carefully and found that the buoyancy flux term is wrongly calculated. As to the LSTIDE, we missed the surface pressure power term, which counts for a large proportion of the tidal energy. As requested, we also calculated the horizontal viscous dissipation and added this to the table. We demonstrate the derivation and calculation of the kinetic energy budget in the Appendix A1 of the revised manuscript.

Below Table 1 shows that, from a global integration view, LSTIDE increases bottom drag and viscous dissipation terms by about 1 TW. The 4.5 TW tidal potential power input is mostly balanced by the surface pressure power $-\mathbf{u_h} \cdot \nabla_h (\rho_0 g \eta)$. If we assume a high-resolution run, which involves propagating internal tides, this surface pressure power term would be smaller because internal tides decrease the surface tide amplitudes (Jayne and St. Laurent, 2001). Then this part of energy would be redistributed to buoyancy flux and viscous dissipation terms, depending on how much internal tide energy can be generated.

Jayne, S. R., & St. Laurent, L. C. (2001). Parameterizing tidal dissipation over rough topography. Geophysical Research Letters, 28(5), 811-814.

Table 1: A global integration of kinetic energy budget from the model results. The surface wind stress, bottom stress, vertical viscous dissipation, horizontal viscous dissipation, buoyancy flux, tidal potential power, surface pressure power terms and total kinetic energy are in order listed in the table. The expressions of these terms can be found in the Appendix A1 of the revised manuscript. Note that all except the last term have a unit of TW, while kinetic energy has a unit of $10^{18}\ J$. This table is also added in the revised manuscript.

Experiment ID	wind stress	bott stress	vert visc	horiz visc	buoy flux	tide	surf pressure	KE
NOTIDE	3.11	-0.18	-2.19	-0.17	-0.58	0.00	-0.02	1.30
CVTIDE	3.11	-0.18	-2.19	-0.18	-0.58	0.00	-0.02	1.31
LSTIDE	3.11	-0.85	-2.29	-0.30	-0.58	4.55	-3.51	1.53

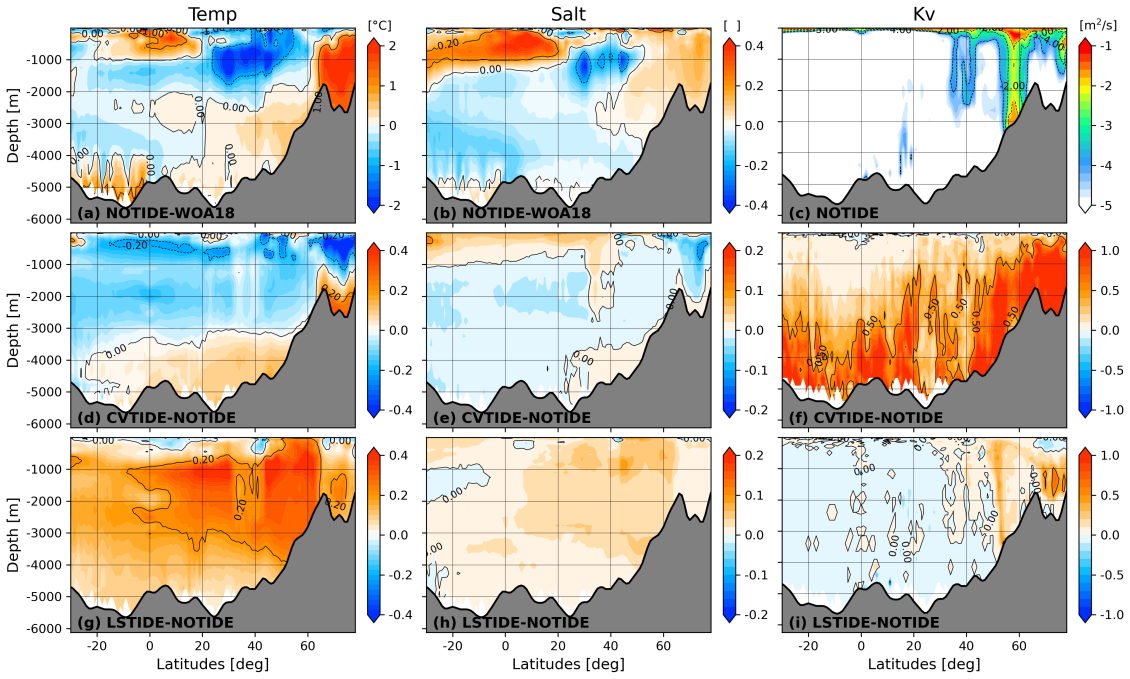

Figure 1: Zonal mean meridional section of the Atlantic hydrography and vertical diffusivity. Note this is calculated with a zonal mean throughout the Atlantic basin. Panel (a) and (b) shows the model bias between NOTIDE and WOA18. The middle and bottom rows show the difference between CVTIDE/LSTIDE and NOTIDE. In the right column, vertical diffusivity is shown in a decimal logarithm scale.

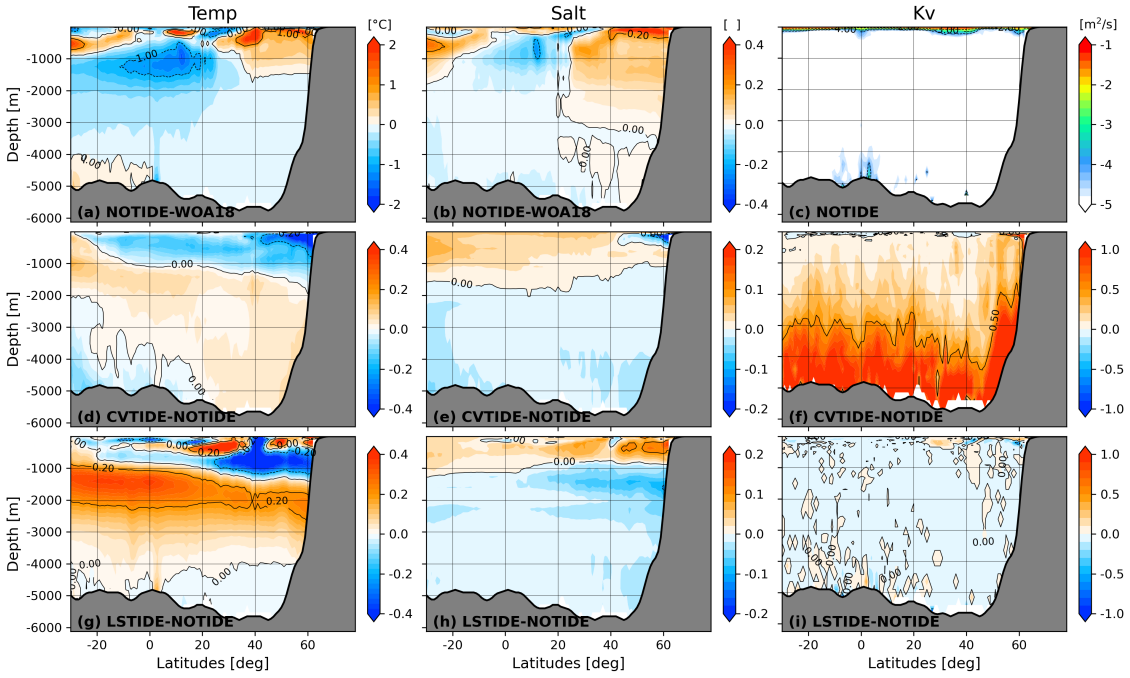

Figure 2: The same as Fig. 1 but in the Indo-Pacific Ocean.

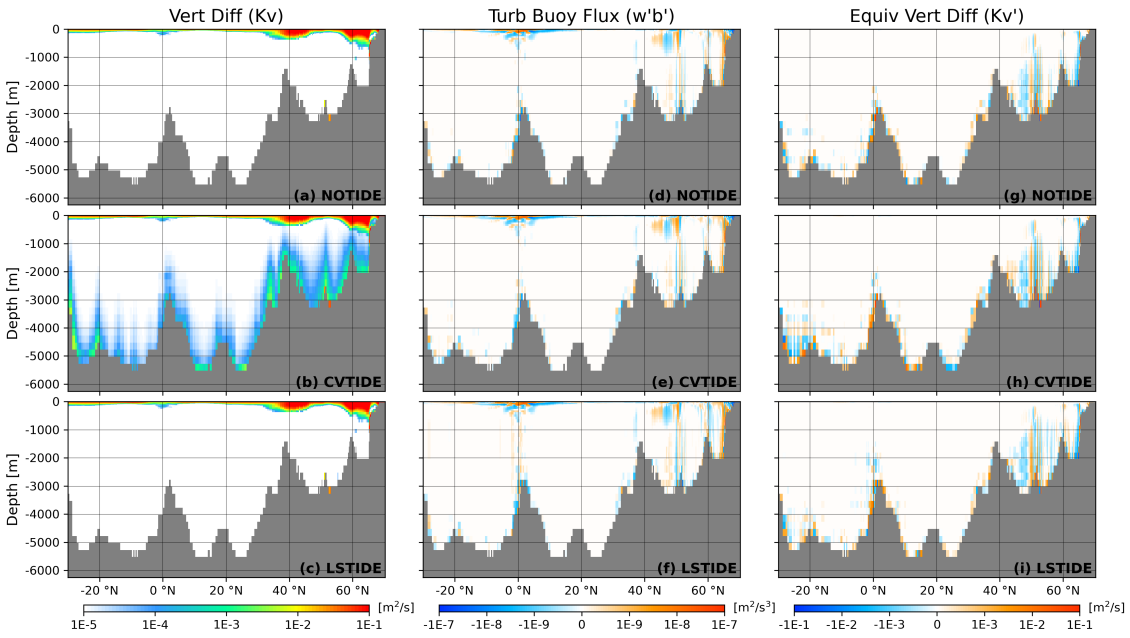

Figure 3: The vertical diffusivity, the turbulent buoyancy flux and its equivalent vertical diffusivity along the transection of 30° W. The calculation of turbulent buoyancy flux and the equivalent vertical diffusivity is introduced in the Appendix A2 of the revised manuscript. All panels are shown in a decimal logarithm scale.

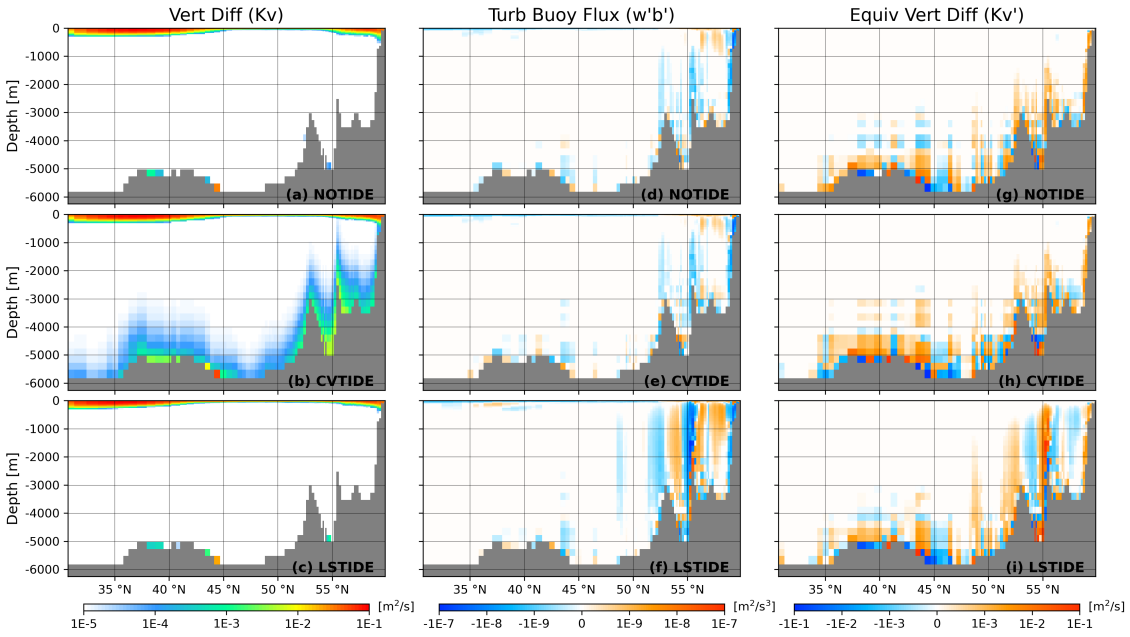

Figure 4: The vertical diffusivity, the turbulent buoyancy flux and its equivalent vertical diffusivity along the transection of 165° E. The calculation of turbulent buoyancy flux and the equivalent vertical diffusivity is introduced in Appendix A2 of the revised manuscript. All panels are shown in a decimal logarithm scale. This figure is also added in the revised manuscript.

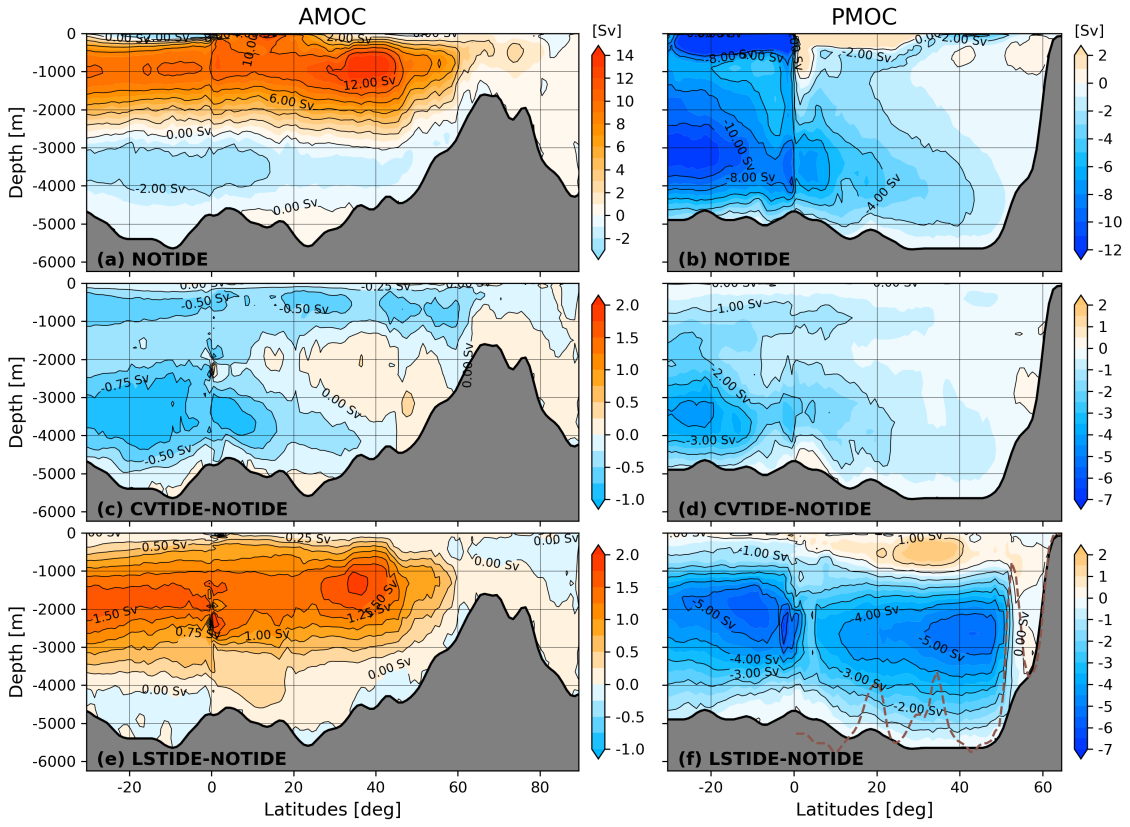

Figure 5: The MOC results in the three sensitivity runs. The upper panel shows the result from the control run, while the other two panels show the difference between CVTIDE/LSTIDE and NOTIDE. The left column and right column represent AMOC and PMOC, respectively. The brown dashed line in panel (f) denotes the North Pacific topography along the 180° transection. This figure is the same as Fig. 11 in the manuscript.